# Journal Pre-proof

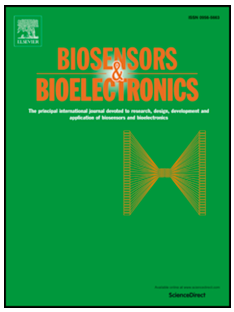


Designing electrochemical interfaces based on nanohybrids of avidin functionalized-carbon nanotubes and ruthenium nanoparticles as peroxidase-like nanozyme with supramolecular recognition properties for site-specific anchoring of biotinylated residues

Pablo Gallay, Marcos Eguílaz, Gustavo Rivas

PII: S0956-5663(19)30843-7

DOI: https://doi.org/10.1016/j.bios.2019.111764

Reference: BIOS 111764

To appear in: *Biosensors and Bioelectronics*

Received Date: 29 April 2019

Revised Date: 1 October 2019

Accepted Date: 3 October 2019

Please cite this article as: Gallay, P., Eguílaz, M., Rivas, G., Designing electrochemical interfaces based on nanohybrids of avidin functionalized-carbon nanotubes and ruthenium nanoparticles as peroxidase-like nanozyme with supramolecular recognition properties for site-specific anchoring of biotinylated residues, *Biosensors and Bioelectronics* (2019), doi: https://doi.org/10.1016/j.bios.2019.111764.

# Designing electrochemical interfaces based on nanohybrids of avidin functionalized-carbon nanotubes and ruthenium nanoparticles as peroxidase-like nanozyme with supramolecular recognition properties for site-specific anchoring of biotinylated residues

**Pablo Gallay, Marcos Eguílaz*, Gustavo Rivas***

**INFIQC. Departamento de Fisicoquímica. Facultad de Ciencias Químicas. Ciudad Universitaria. 5000 Córdoba. Argentina.**

***Corresponding authors**

**e-mail: grivas@fcq.unc.edu.ar; mrubio@fcq.unc.edu.ar**

**Phone number: +54-351-45353866; Fax number: +54-351-4334188.**

**ABSTRACT**

We are reporting an original supramolecular architecture based on a rationally designed new nanohybrid with enhanced peroxidase-like activity and site-specific biorecognition properties using avidin-functionalized multi-walled carbon nanotubes (MWCNTs-Av) and Ru nanoparticles (RuNPs). The nanohybrid-electrochemical interface was obtained by drop-coating of MWCNTs-Av dispersion at glassy carbon electrodes (GCE) followed by solvent evaporation and further electrodeposition of RuNPs (50 ppm $RuCl_2$ for 15 seconds at -0.600 V). The simultaneous presence of MWCNTs and RuNPs produces a synergic effect on the non-enzymatic catatalytic reduction of $H_2O_2$ and allows the quantification of $H_2O_2$ in a wide linear range (from 5.0 x $10^{-7}$ M to 1.75 x $10^{-3}$ M) with a low limit of detection (65 nM). The avidin residues present in MWCNTs-Av/RuNPs hybrid nanomaterial allowed the anchoring by bioaffinity of biotinylated glucose oxidase (biot-GOx) as proof-of-concept of the analytical application of MWCNTs-Av platform for biosensors development. The resulting nanoarchitecture behaves as a bienzymatic-like glucose biosensor with a competitive analytical performance: linear range between 2.0 x $10^{-5}$ M and 1.23 x $10^{-3}$ M, sensitivity of (0.343 ± 0.002) µA $mM^{-1}$ or (2.60 ± 0.02) µA $mM^{-1}$ $cm^{-2}$, detection limit of 3.3 µM, and reproducibility of 5.2 % obtained with five different GCE/MWCNTs-Av/RuNPs/biot-GOx bioplatforms prepared the same day using the same MWCNTs-Av dispersion, and 9.1% obtained with nine biosensors prepared in different days with nine different MWCNTs-Av dispersions. The average concentrations of glucose in Gatorade®, Red bull® and Pepsi® with the biosensor demonstrated excellent agreement with those reported in the commercial beverages.

**Keywords: MWCNTs-functionalization; Ruthenium nanoparticles; Avidin; Nanozyme; Glucose Oxidase; Supramolecular recognition.**

## 1. INTRODUCTION

One of the most important challenges in the development of electrochemical biosensors is to obtain platforms that allow the robust immobilization of the biorecognition molecules and a sensitive, selective and fast transduction of the biorecognition event (Maduraiveeran et al., 2018; Zhu et al., 2015).

Recently, nanomaterial-based artificial enzymes (named “nanozymes”) have emerged as the next generation enzyme-mimics with important advantages such as ease and low-cost mass-production, robustness to work in harsh environments, and high stability, compared to the intrinsic shortcomings of natural enzymes (high cost for purification, low stability, and limitations in storage and reusing) (Wei and Wang, 2013; Wu et al., 2019). Since the discovery of peroxidase-like activity of $Fe_3O_4$ nanoparticles in 2007 (Gao et al., 2007), several nanomaterials have emerged as nanozymes with intrinsic peroxidase-like activities (Attar et al., 2019). The unique physicochemical properties of nano-sized materials like high surface-to-volume ratio, catalytic activity, biocompatibility and easy functionalization endow nanozymes with multiple functionalities and provide interesting possibilities for the rational design of high-performance electrochemical interfaces with interesting (bio)sensing applications (Golchin et al., 2017). Moreover, the possibility of tailor-made design of nanomaterials with specific properties by rational manipulation of their composition and functionalities represents an interesting

alternative for the development of novel multifunctional nanozymes systems (Wu et al., 2018).

Biosensing devices prepared with innovative hybrid materials constituted by two or more components have attracted great attention as they have shown improved properties compared to the individual components due to the combined properties and/or synergistic effect of the individual materials. For example, hybrid materials based on carbon nanotubes (CNTs) combined with other carbon-based nanomaterials (Bai et al., 2016; Wang et al., 2017), and metallic (Liu and Ding, 2017; Zhang et al., 2018) or metal oxides (Shahnavaz and Abd Hamid, 2017) nanoparticles have shown improved peroxidase-like activities compared to the individual components.

CNTs functionalization has demonstrated to be a critical aspect when developing electrochemical (bio)sensors. In fact, it is absolutely necessary to functionalize the nanostructures, either covalently or non-covalently, to be able to manipulate them and to allow their incorporation at the electrochemical transducers. Among the different schemes used to functionalize the nanostructures, the use of biological molecules with particular biorecognition properties, like glucose oxidase (Gutierrez et al., 2012), cytochrome c (Eguílaz et al., 2016), calf-thymus double stranded DNA (Primo et al., 2014, 2013), and cysteine (Gutierrez et al., 2017), has proved to be highly advantageous. Recently (Gutierrez et al., 2019), we have proposed the non-covalent functionalization of MWCNTs with avidin (MWCNTs-Av) as a building block to obtain a multifunctional analytical platform with successful application for hydrogen peroxide biosensing by anchoring the biotinylated horseradish

peroxidase at glassy carbon electrodes (GCE) modified with the MWCNTs-Av dispersion.

In this work, we report for the first time the preparation of a hybrid material with enhanced peroxidase-like activity and supramolecular recognition properties, based on the rational combination of avidin-functionalized multi-walled carbon nanotubes and ruthenium nanoparticles (RuNPs). In the following sections we discuss the catalytic activity of MWCNTs-Av/RuNPs nanohybrid towards hydrogen peroxide, the optimization of the experimental conditions for the bienzymatic-like glucose biosensing through the site-specific immobilization of biotinylated glucose oxidase (biot-GOx), and the analytical performance of the resulting biosensor.

## 2. EXPERIMENTAL

### 2.1. Chemicals and solutions

Glucose oxidase (GOx) (from Aspergillus niger, EC 1.1.3.4, 163,400 units/g of solid) and ruthenium atomic absorption standard solution (1010 μg $mL^{-1}$ in 5 % HCl) were purchased from Sigma. Carbon nanotubes (MWCNTs, (30 ± 15) nm diameter, (1 – 5) μm length, purity > 95%), were supplied from Nanolab (USA). $NaH_2PO_4$ and $Na_2HPO_4$ were received from Baker. β-D-(+)-glucose was obtained from Merck. EZ-Link™ NHS-LC-Biotin and avidin (from egg white) were purchased from Thermo Fisher Scientific. Gel filtration Column-Sephadex® G-25M was purchased from Sigma. Other chemicals were of analytical grade and used without further purification. The supporting electrolyte was a 0.050 M phosphate buffer solution pH 7.40. Ultrapure water (ρ = 18.2 MΩ cm) from a Millipore-MilliQ system was used for preparing all aqueous solutions.

## 2.2. Apparatus

Sonication treatments were performed with a VCX 130W ultrasonic processor (Sonics and Materials, Inc.), of 20 kHz frequency with a titanium alloy microtip (3 mm diameter).

Scanning electron microscopy (SEM) pictures were obtained with a field emission gun scanning electron microscope (FE-SEM, Zeiss, ΣIGMA model) equipped with secondary and back-scattered electron detectors. The samples were prepared by dropping the dispersion onto GCE disks followed by the evaporation of the solvent.

UV-vis absorption spectra were obtained with a Shimadzu UV-1700 Pharma spectrophotometer using a quartz cell of 1 mm path length.

Electrochemical experiments were carried out with a TEQ_04 potentiostat. Bare glassy carbon (GCE, CH Instruments, 3mm diameter) and modified GCE were used as working electrodes. A platinum wire and a Ag/AgCl, 3 M NaCl (BAS) were used as auxiliary and reference electrodes, respectively. All potentials are referred to this reference electrode. The electroactive areas of the electrodes were performed by cyclic voltammetry using hydroquinone solution as redox probe.

## 2.3. Preparation of biotinylated GOx

A 10.0 mg $mL^{-1}$ GOx solution (prepared in 0.050 M phosphate buffer solution pH 7.40) was mixed with 300.0 µL of NHS-LC-Biotin reagent (4.4 mg $mL^{-1}$, prepared in DMSO) and incubated for 24 h at 4 ºC. biot-GOx was purified by gel filtration with Sephadex G-25 following the procedure described by the

supplier. The concentration of biot-GOx, obtained from the maximum absorbance of FAD band, was 3.0 mg $mL^{-1}$.

## 2.4. Preparation of the nanohybrid bioplatform (GCE/MWCNTs-Av/RuNPs/biot-GOx)

### *2.4.1. Preparation of MWCNT-Av dispersion*

MWCNTs-Av dispersion was obtained by mixing 0.50 mg of MWCNTs with 1.0 mL of avidin solution (1.0 mg $mL^{-1}$ prepared in 50:50 v/v, ethanol/water) followed by sonication with a sonicator probe for 5.0 min. The amplitude was 50% and the sample was kept in an ice-bath during the procedure.

### *2.4.2. Construction of GCE/MWCNTs-Av/RuNPs*

Before modification, the GCEs were first polished with alumina slurries of 1.0, 0.3 and 0.05 μm for 1.0 min each, rinsed thoroughly with deionized water, sonicated for 5 s in water, and finally dried under a nitrogen stream. GCE/MWCNT-Av was prepared by casting 20 μL of the MWCNT-Av dispersion onto the glassy carbon surface and drying at room temperature. RuNPs were electrodeposited at GCE/MWCNTs-Av surface by applying a constant potential of -0.600 V for 15 s in a 50 ppm ruthenium solution under stirring conditions. Subsequently, the GCE/MWCNTs-Av/RuNPs electrode was exhaustively rinsed with water.

### *2.4.3. Immobilization of biot-GOx at GCE/MWCNTs-Av/RuNPs (GCE/MWCNTs-Av/RuNPs/biot-GOx)*

GCE/MWCNTs-Av/RuNPs/biot-GOx bioplatform was obtained by drop-coating a 20 µL-aliquot of 3.0 mg $mL^{-1}$ biot-GOx onto GCE/MWCNTs-Av/RuNPs for 1 h under conditions that avoiding solvent evaporation. Finally, GCE/MWCNTs-Av/RuNPs/biot-GOx was rinsed by immersion in a 0.05% Tween-20 solution (prepared in a 0.050 M buffer phosphate solution pH 7.40) for 5 s and in a 0.050 M buffer phosphate solution pH 7.40 for 5 s. As control, GCE/MWCNTs-Av/RuNPs/GOx was prepared under similar experimental conditions using non-biotinylated GOx.

### 2.5. Procedure

Cyclic voltammetry experiments were carried out between 0.400 V and -0.400 V at a scan rate of 0.100 $Vs^{-1}$. Amperometric experiments were performed in stirred solutions at -0.050 V. All electrochemical experiments were conducted at room temperature in a 0.050 M phosphate buffer solution pH 7.40.

### 2.5. Determination of glucose in soft drink samples

Commercial soft drinks (Pepsi®, Gatorade® and Red Bull®), obtained from a local drugstore, were used to evaluate the real application of the proposed nanohybrid glucose biosensor. A 10 µL-aliquot of soft drinks was directly transferred to the electrochemical cell containing 5.0 mL of 0.050 M phosphate buffer solution pH 7.40, and the determination of glucose was performed by amperometry at -0.050 V using the standard additions method in all cases.

## 3. RESULTS AND DISCUSSION

### 3.1. Characterization of GCE/MWCNTs-Av/RuNPs

Figure 1 shows the different steps involved in the modification of GCE with MWCNTs-Av and RuNPs and further construction of a GOx-based biosensor through protein supramolecular complex formation by site-specific avidin-biotin interactions.

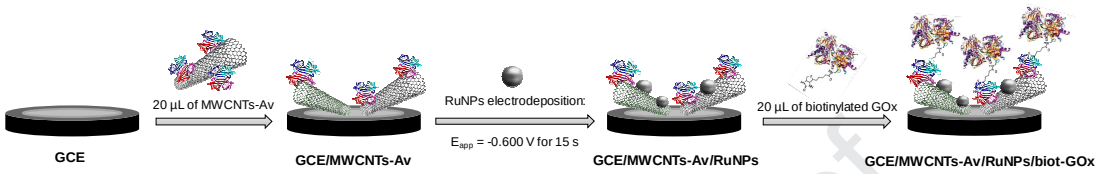


**Figure 1:** Schematic display of the steps involved in the preparation of the GCE/MWCNTs-Av/RuNPs/biot-GOx biosensor.

GCE modified with MWCNTs-Av/RuNPs nanohybrid material was prepared in two steps. First, MWCNTs were non-covalently functionalized with avidin and deposited on the electrode surface. The resulting GCE/MWCNTs-Av was further decorated with RuNPs by deposition at -0.600 V for 15 s to build the nanohybrid platform denoted as GCE/MWCNTs-Av/RuNPs.

SEM images of the resulting GCE/MWCNTs-Av shows an excellent coverage of the whole surface (Figure 2A). After the deposition of Ru, there is an important number of aggregates of RuNPs in intimate contact with the nanotubes (Figure 2B).

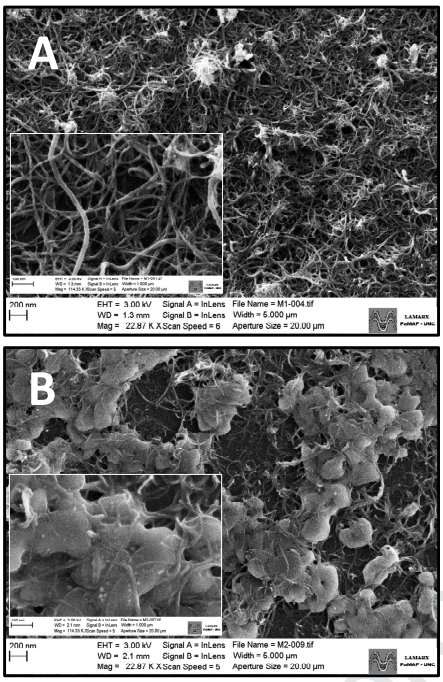


**Figure 2:** SEM micrographs of (A) GCE/MWCNTs-Av and (B) GCE/MWCNTs-Av/RuNPs. Magnification: 22870 x. The insets correspond to pictures of the same electrodes with higher magnification (114330 x).

It is important to remark that the coverage of RuNPs is not complete, leaving avidin residues exposed for the interaction with biot-GOx. As it will be discussed in the following section, the coverage of Ru was a critical parameter to obtain a catalytic surface able to be functionalized with biot-GOx.

Peroxidase-like properties of MWCNTs-Av/RuNPs hybrid nanomaterial were studied by cyclic volmmetry using hydrogen peroxide as redox marker. Figure 3A shows cyclic voltammograms for 0.050 M $H_2O_2$ obtained at GCE (a), GCE/MWCNTs-Av (b), GCE/RuNPs (c), GCE/MWCNTs-Av/RuNPs (d), and GCE/RuNPs/MWCNTs-Av (e).

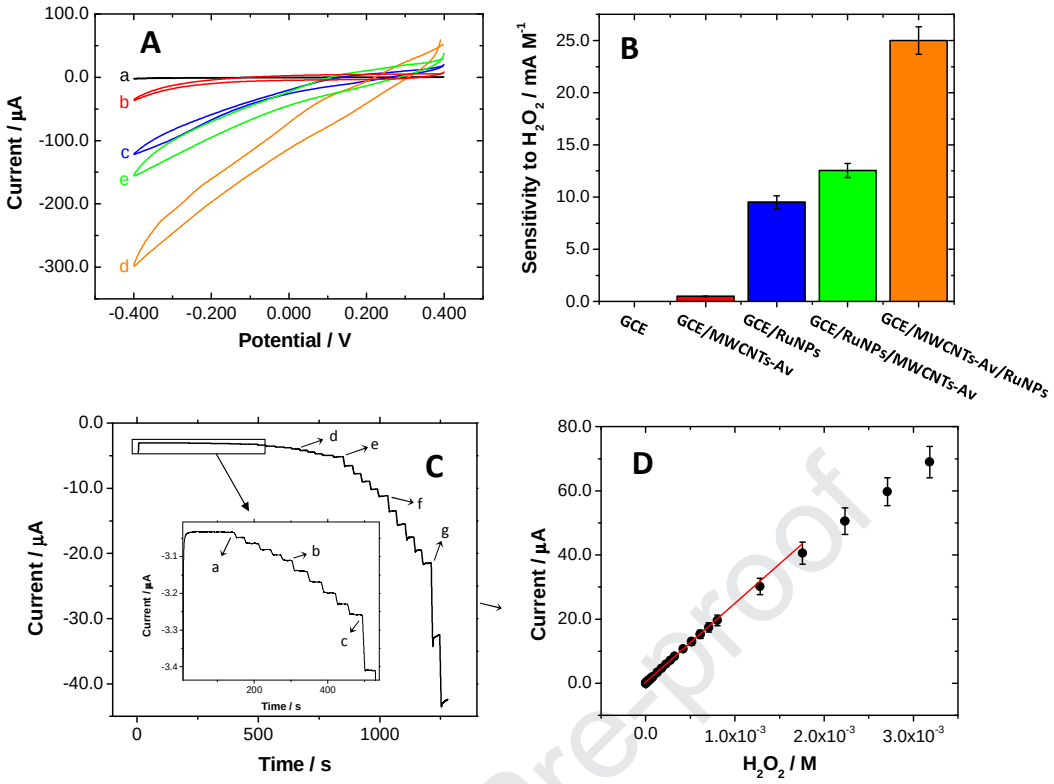


**Figure 3:** (A) Cyclic voltammograms of 0.050 M $H_2O_2$ obtained at GCE (a), GCE/MWCNTs-Av (b), GCE/RuNPs (c), GCE/MWCNTs-Av/RuNPs (d), and GCE/RuNPs/MWCNTs-Av (e). v=0.100 V $s^{-1}$. (B) Sensitivity towards $H_2O_2$ obtained from amperometric experiments at -0.050 V at GCE, GCE/MWCNTs-Av, GCE/RuNPs, GCE/RuNPs/MWCNTs-Av and GCE/MWCNTs-Av/RuNPs. (C) Amperometric recording obtained at GCE/MWCNTs-Av/RuNPs for successive additions of 5.0 x $10^{-7}$ M (a), 1.0 x $10^{-6}$ M (b), 5.0x$10^{-6}$ M (c), 1.0 x $10^{-5}$ M (d), 5.0 x $10^{-5}$ M (e), 1.0x$10^{-4}$ M (f) and 5.0x$10^{-4}$ M $H_2O_2$ (g). (D) Calibration plot obtained from the amperometric recording shown in Figure 3C. Working potential: -0.050 V. Supporting electrolyte: 0.050 M phosphate buffer solution pH 7.40.

At bare GCE (a), as expected, the reduction of $H_2O_2$ is negligible (Eguílaz et al., 2014). The presence of MWCNTs at GCE/MWCNTs-Av produced a

decrease in the overvoltage for $H_2O_2$ reduction and an increase of the associated currents (b). This catalytic effect is more pronounced at GCE/RuNPs (c) due to the known electrocatalytic activity of Ru towards the reduction of $H_2O_2$ (Sakslund et al., 1995; Ye et al., 2016). More interestingly, at GCE/MWCNTs-Av/RuNPs (d) there is a remarkable increase in the reduction current due to the larger electroactive surface and a synergism between MWCNTs and RuNPs. Similar synergic effects for $H_2O_2$ reduction have been reported in the case of hybrid materials based on MWCNTs/ferrites (Gutierrez et al., 2018), MWCNTs/carbon dots (Bai et al., 2016), and MWCNTs/graphene oxide/platinum nanoparticles (Wang et al., 2014). Compared to GCE/MWCNTs-Av/RuNPs, the reduction currents are smaller at GCE/RuNPs/MWCNTs-Av (e) probably due to a lower accesibility of RuNPs behind the MWCNTs-Av layer, as well as a less efficient deposition of MWCNTs-Av at Ru-modified surface, compared to GCE. Similar behavior was observed for the different electrodes by amperometry at -0.050 V (Figure 3B). In fact, sensitivities to $H_2O_2$ of (0.49 ± 0.02) mA $M^{-1}$, (9.5 ± 0.6) mA $M^{-1}$, (12.6 ± 0.7) mA $M^{-1}$ and (25 ± 1) mA $M^{-1}$, were obtained at GCE/MWCNTs-Av, GCE/RuNPs, GCE/RuNPs/MWCNTs-Av and GCE/MWCNTs-Av/RuNPs, respectively. These results confirm the synergism between MWCNTs and RuNPs since the sensitivity to $H_2O_2$ obtained at GCE/MWCNTs-Av/RuNPs is higher than the addition of the sensitivities obtained separately at GCE/MWCNTs-Av and GCE/RuNPs. Therefore, the rational combination of MWCNTs-Av with RuNPs produced a greatly enhanced electrochemical performance for $H_2O_2$ reduction at GCE/MWCNTs-Av/RuNPs, demonstrating the efficient activity of the nanobiocomposite as peroxidase-mimic. Figure 3C displays the amperometric response of $H_2O_2$ at -0.050 V

obtained at GCE/MWCNTs-Av/RuNPs. A fast response, with steady-currents reached in 5 s is obtained after each addition of $H_2O_2$. The corresponding calibration plot is shown in Figure 3D. A very wide linear range, of almost four orders of magnitude, was obtained with the nanohybrid-modified electrode (5.0 x $10^{-7}$ M – 1.75 x $10^{-3}$ M), with a sensitivity of (25.4 ± 0.1) μA $mM^{-1}$ ($r^2$ = 0.998) (or (113.9 ± 0.4) μA $mM^{-1}$ $cm^{-2}$)), and a limit of detection of 65 nM (taken as 3.3 σ/S, where σ is the standard deviation of the blank signal and S the sensitivity (Olivieri and Goicoechea, 2007)). No interference of oxygen was observed under out experimental conditions since calibrations plots performed in the absence and presence of oxygen gave similar sensitivities ((24 ± 2) μA $mM^{-1}$ and (25.4 ± 0.1) μA $mM^{-1}$, respectively). It is important to remark that the proposed GCE/MWCNTs-Av/RuNPs sensor shows a wider linear range than that obtained with the enzymatic $H_2O_2$ biosensor based on MWCNTs-Av and biotinylated HRP using hydroquinone as external redox mediator (1.0 x $10^{-6}$ M – 1.4 x $10^{-5}$ M) (Gutierrez et al., 2019). Table 1-SI compares the analytical performance of our $H_2O_2$ sensor with those of other sensors based on hybrid materials with peroxidase-like activity reported in recent years. The proposed $H_2O_2$ sensor possesses an excellent limit of detection which is lower than those obtained with hybrid materials based on CNTs and carbon dots (0.25 μM) (Bai et al., 2016), oxygen-doped nitrogen-rich carbon nanoribbons polymer (0.51 μM) (Wang et al., 2017), zinc chromite nanoparticles (0.11 μM) (Shahnavaz and Abd Hamid, 2017), or metal-organic framework (0.7 μM) (Wang et al., 2019); and comparable to that obtained with a nanohybrid microelectrode based on carbon fiber wrapped by gold nanoparticles decorated nitrogen-doped carbon nanotube arrays (0.05 μM) (Zhang et al., 2018). $H_2O_2$ sensors based on hybrid

materials of reduced graphene oxide decorated with trimetallic Au-Pt-Pd nanoparticles (Dong et al., 2018) and Au-Pt alloy microspheres (Bai et al., 2018) showed a one-order lower limit of detection.

### 3.2. Optimization of GCE/MWCNTs-Av/RuNPs/biot-GOx for the quantification of glucose

Based on the excellent biorecognition properties of the avidin that supports the MWCNTs (Gutierrez et al., 2019), we compared the electrochemical response to glucose of GCE/MWCNTs-Av/RuNPs modified with biotinylated and non-biotinylated GOx, selected as model enzyme (GCE/MWCNTs-Av/RuNPs/biot-GOx and GCE/MWCNTs-Av/RuNPs/GOx, respectively). Amperometric experiments performed at -0.050 V for successive additions of 5.0 x $10^{-5}$ M glucose showed that the response at GCE/MWCNTs-Av/RuNPs/biot-GOx was 5.6 times higher than that obtained at GCE/MWCNTs-Av/RuNPs/GOx (Figure 1-SI). These results confirm that GCE/MWCNTs-Av/RuNPs platform allows stable immobilization of the biotinylated enzyme through the formation of a high-affinity supramolecular complexe by site-specific avidin-biotin interactions, opening the doors to the development of other biosensing platforms.

The electrodeposition time of Ru at GCE/MWCNTs-Av demonstrated to be a critical parameter for the construction of the biosensor. Figure 4 shows the effect of Ru electrodeposition time on the amperometric response of $H_2O_2$ (A) and glucose (B) obtained at GCE/MWCNTs-Av/RuNPs and GCE/MWCNTs-Av/RuNPs/biot-GOx, respectively.

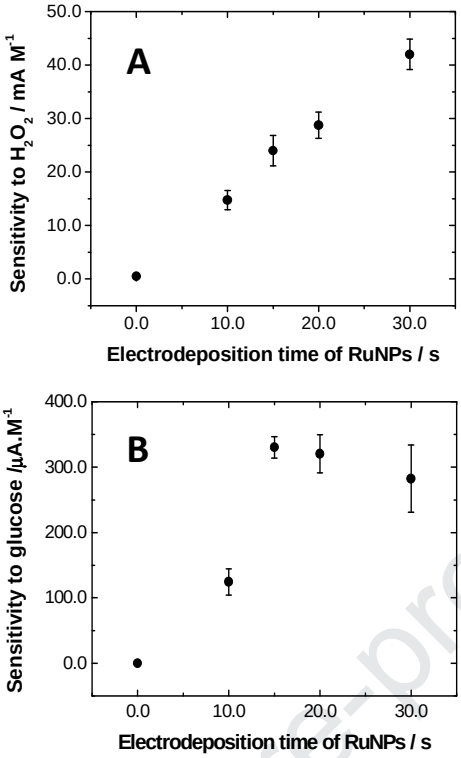


**Figure 4:** Influence of the Ru electrodeposition time on the sensitivity to (A) $H_2O_2$ obtained at GCE/MWCNTs-Av/RuNPs, and (B) glucose obtained at GCE/MWCNTs-Av/RuNPs/biot-GOx, from amperometric experiments at -0.050 V. Supporting electrolyte: 0.050 M phosphate buffer solution pH 7.40.

The continuous increase in sensitivity for $H_2O_2$ reduction in the whole evaluated range of Ru electrodeposition time demonstrates the importance of the amount of the nanozyme electrodeposited at GCE/MWCNTs-Av on the electrocatalytic reduction of $H_2O_2$ (Figure 4A). However, the sensitivity to glucose increases with Ru electrodeposition time up to 15 s and levels off thereafter (Figure 4B), due to the blockage of the avidin sites for further supramolecular recognition of biotinylated GOx. Thus, an electrodeposition time of Ru of 15 s was selected for the preparation of the bioanalytical platform.

Figure 5A displays the amperometric response of glucose at -0.050 V obtained at GCE/MWCNTs-Av/RuNPs/biot-GOx under the optimal conditions.

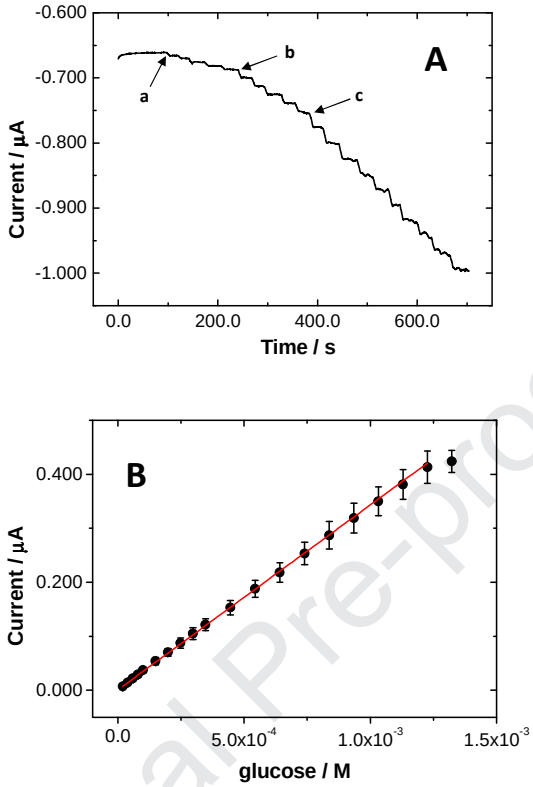


**Figure 5:** (A) Amperometric recording obtained at GCE/MWCNTs-Av/RuNPs/biot-GOx for successive additions of 2.0 x $10^{-5}$ M (a), 5.0 x $10^{-5}$ M (b), and 1.0x$10^{-4}$ M glucose (c). (B) Calibration plot obtained from the amperometric recording shown in Figure 5A. Working potential: -0.050 V. Supporting electrolyte: 0.050 M phosphate buffer solution pH 7.40.

A clearly defined and fast response is observed after each addition of glucose, with steady-state currents reached in 6 s. The corresponding calibration plot displayed in Figure 5B shows an almost two-orders linear range from 2.0 x $10^{-5}$ M to 1.23 x $10^{-3}$ M, with a sensitivity of (0.343 ± 0.002) µA $mM^{-1}$ or (2.60 ± 0.02) µA $mM^{-1}$ $cm^{-2}$ ($r^2$ = 0.9995), and a limit of detection of 3.3 µM (calculated as it was previously indicated). Table 1 shows the comparison of the

analytical performance of our glucose biosensor with the most relevant biosensors reported since 2016 operating at potential able to produce the reduction of the enzymatically generated hydrogen peroxide.

**Table 1:** Comparison of the analytical characteristics obtained with different GOx-based biosensors.

| ELECTROCHEMICAL BIOPLATFORMS FOR GLUCOSE BIOSENSING | | | | | |
|---|---|---|---|---|---|
| **Platform** | **Detection** | **Linear Range** | **Sensitivity** | **LOD** | **Ref.** |
| GCE/MWCNTs-PEG/IL/GOx/Naf | Amp. (-0.270 V) | (20 – 950) μM | -- | 0.2 μM | (Ning et al., 2019) |
| GCE/(MWCNTs-Cyt c/GOx)$_2$/Naf | Amp. (-0.050 V) | (100 – 1000) μM | 0.096 μA mM$^{-1}$ | 8 μM | (Eguílaz et al., 2016b) |
| GCE/CNTs/HRP-GOx/Naf | CV | (22 – 7000) μM | 5.14 μA mM$^{-1}$ cm$^{-2}$ | 7 μM | (Yang et al., 2017) |
| Stainless-steel Pin/MWCNTs/ferrocyanide-HRP-GOx | Amp. (-0.200 V) | (50 – 1000) μM | 1.44 μA mM$^{-1}$ | 30 μM | (Rama et al., 2017) |
| KSC/NCNTs/GOx | CV | (5.8 – 18000) μM | 29.4 μA mM$^{-1}$ cm$^{-2}$ | 1.9 μM | (Song et al., 2016) |
| GMFE/$TiO_2$NRs/GOx-CS | Amp. (-0.500 V) | Up to 1500 μM | 18.6 μA mM$^{-1}$ cm$^{-2}$ | 2.2 μM | (Zhang et al., 2016) |
| GCE/HNF-$TiO_2$/GOx | Amp. (-0.450 V) | (2 – 3170) μM | 32.6 μA mM$^{-1}$ cm$^{-2}$ | 0.8 μM | (Guo et al., 2017) |
| SPCE/ERGO/IL-CHO/GOx | Amp. (-0.450 V) | (50 – 2400) μM | 17.7 μA mM$^{-1}$ cm$^{-2}$ | 17 μM | (Manoj et al., 2018) |
| AuE/GNS-PEI-AuNPs/GOx | Amp. (-0.350 V) | (1 – 100) μM | 93 μA mM$^{-1}$ cm$^{-2}$ | 0.32 μM | (Rafighi et al., 2016) |
| GCE/TCNFs-GOx | Amp. (-0.550 V) | (13 – 10500) μM | 628.82 μA mM$^{-1}$ cm$^{-2}$ | 3.7 μM | (Guo et al., 2018) |
| AuE/PEDOT-PSS/(CS-NGr-GOx)$_2$ | Amp. (-0.200 V) | (100 – 1400) μM | 237 μA mM$^{-1}$ cm$^{-2}$ | 41 μM | (David et al., 2018) |
| GCE/$Fe_3O_4$-PB/GOx-BSA/GA | Amp. (-0.150 V) | (5 – 1200) μM | 32 μA mM$^{-1}$ cm$^{-2}$ | 0.5 μM | (Jomma et al., 2016) |
| PGE/CdS-ZnS-QDs/GOx | Amp. (-0.500 V) | (10 – 1000) μM | 11.5 μA mM$^{-1}$ cm$^{-2}$ | 3 μM | (Saglam et al., 2016) |
| GCE/AuNFs/GNS-IL-AuNRs(sol-gel)/GOx/GA/Naf | Amp. (-0.200 V) | (1 – 764) μM | 0.06408 μA mM$^{-1}$ | 0.38 μM | (Tang et al., 2019) |
| GCE/$CaTiO_3$NPs-GOx-CS | Amp. (-0.450 V) | (7 – 1490) μM | 14.1 μA mM$^{-1}$ cm$^{-2}$ | 2.3 μM | (L. Wang et al., 2017) |
| CPE-TSA-Ag@Zn/GOx/IL | Amp. (-0.450 V) | (2 – 1022) μM | -- | 0.8 μM | (Dong et al., 2016) |
| GCE/KB/HRP-GOx-GA | Amp. (-0.100 V) | (5 – 1500) μM | 330 μA mM$^{-1}$ cm$^{-2}$ | 2 μM | (Xia et al., 2017) |
| AuE/SAMs/HRP-GOx/AuNPs/4-amino thiophenol | CV | (16.5 – 10000) μM | 41.78 μA mM$^{-1}$ cm$^{-2}$ | 5.4 μM | (Gong et al., 2016) |
| GCE/MWCNTs-Av/RuNPs/biot-GOx | Amp. (-0.050 V) | (20 – 1230) μM | 0.343 μA mM$^{-1}$ (2.60 μA mM$^{-1}$ cm$^{-2}$) | 3.3 μM | This work |

GCE: glassy carbon electrode; MWCNTs: multi-walled carbon nanotubes; PEG: polyethylene glycol; IL: ionic liquid; GOx: glucose oxidase; Naf: nafion; Cyt c: cytochrome c; CNTs: carbon nanotubes; HRP: horseradish peroxidase; KSC: Kenaf Stem-derived porous carbón; NCNTs: nitrogen-doped carbon nanotubes; GMFE: graphite microfiber electrode; $TiO_2$NRs: $TiO_2$ nanorods; CS: chitosan; HNF: hollow nanofibers; SPCE: screen-printed carbon electrode; ERGO: electrochemically reduced graphene oxide; IL-CHO: aldehyde functionalized ionic liquid; AuE: gold electrode; GNS: Graphene nanosheets; PEI: polyethylenimine; AuNPs: gold nanoparticles; TCNFs: titanium carbide-carbon nanofibers; PEDOT: poly(3,4-ethylenedioxythiophene); PSS: poly(styrene sulfonate); NGr: nitrogen doped graphene; PB: Prussian blue; BSA: bovine serum albumin; GA: glutaraldehyde; PGE: pencil graphite electrode; QDs: quantum dots; AuNFs: gold nanoflowers; AuNRs: gold nanorods; $CaTiO_3$NPs: perovskite-type calcium titanate nanoparticles; CPE: carbon paste electrode; TSA-Ag@Zn: thiosalicylic acid metal-organic framework; KB: Ketjen Black; SAMs: self-assembled monolayers

The limit of detection is comparable or lower than most of them. Glucose biosensors based on the immobilization of GOx onto electrode surfaces modified with metal-organic framework (Dong et al., 2016) and magnetite-prussian blue (Jomma and Ding, 2016) nanocomposites, graphene-

polyethylenimine-gold nanohybrid (Rafighi et al., 2016), MWCNTs, polyethylene glycol and ionic liquid (Ning et al., 2019), porous $TiO_2$ hollow nanofibers (Guo et al., 2017), and a 3D network material of gold nanoflowers, ionic liquid-modified graphene and gold nanorods (Tang et al., 2019) showed a one-order lower limit of detection. Despite the sensitivity is smaller than most of the biosensors showed in Table 1, our biosensor works at potentials considerably less negative than most of them and the linear range and detection limit are very competitive. It is important to mention that even when the sensitivity is smaller at the selected working potential, under these experimental conditions it was possible to obtain a fast stabilization of the base line, a low level of noise and, consequently, a low detection limit.

The reproducibility obtained with five different GCE/MWCNTs-Av/RuNPs/biot-GOx bioplatforms prepared the same day using the same MWCNTs-Av dispersion was 5.2%, while the reproducibility obtained with nine biosensors prepared in different days with nine different MWCNTs-Av dispersions was 9.1%.

The selectivity of GCE/MWCNTs-Av/RuNPs/biot-GOx was evaluated in the presence of other sugars such as lactose, galactose, fructose and maltose (all of them $1.0 \times 10^{-4}$ M). As can be seen in Figure 2A-SI, no interference for the determination of $1.0 \times 10^{-4}$ M glucose was observed in any case. Figure 2B-SI shows the effect of the addition of ascorbic acid and uric acid on the amperometric response of glucose. No interference was observed under the experimental conditions.

To evaluate the real application of the nanohybrid bioplatform, we quantified glucose in different soft drink beverages. The average concentrations of

glucose, obtained from 5 determinations, were (2.5 ± 0.1) g/100 mL, (3.4 ± 0.2) g/100 mL and (4.1 ± 0.2) g/100 mL for Gatorade®, Red bull® and Pepsi® samples, respectively, values that are in excellent agreement with those reported in the commercial beverages (2.4, 3.6 and 3.9 g/100 mL, respectively). These results confirmed the analytical usefulness of GCE/MWCNTs-Av/RuNPs nanohybrid platform for the development of electrochemical biosensors through the association of the electrocatalytic activity of MWCNTs/RuNPs hybrid, and the supramolecular recognition between the avidin that supports the MWCNTs and the biotinylated biorecognition element, in this case exemplified with biotinylated GOx and glucose quantification in soft drinks beverages.

## 4. CONCLUSIONS

We proposed an innovative and original avenue for designing a bioanalytical platform based on the use of a nanohybrid material that allows the site-specific recognition of the biosensing molecule and an efficient (bio)catalytic activity. We built a bienzymatic-like biosensor that involves the use of a nanohybrid constituted by MWCNTs dispersed in avidin, to drive the interaction with biotinylated glucose oxidase used as proof-of-concept, and Ru nanoparticles as peroxidase-like-nanozyme. The resulting pseudo-bienzymatic glucose biosensing nanoarchitecture demonstrated to be sensitive, selective and robust, with successful application in real samples. The new platform represents an interesting alternative for the simple, easy and fast preparation of other biosensors just by a judicious selection of the nanomaterials and the biorecognition and transduction events.

**ACKNOWLEDGEMENTS**

The authors thank CONICET (PIP 2016), SECyT-UNC (2018-2021) and ANPCyT (PICT-2016-1261) for the financial support; and Dr. Fabiana Gutierrez, Dr. María D. Rubianes (INFIQC-UNC), Dr. Gabriela Paglini and Biol. Guillermo Fernandez (Neurophisiology Laboratory, Mercedes and Martín Ferreyra Medical Research Institute) for the preparation of biotinylated GOx. P. G. thanks CONICET for the fellowship.

**REFERENCES**

Amanulla, B., Palanisamy, S., Chen, S.M., Velusamy, V., Chiu, T.W., Chen, T.W., Ramaraj, S.K., 2017. J. Colloid Interface Sci. 487, 370–377.

Attar, F., Shahpar, M.G., Rasti, B., Sharifi, M., Saboury, A.A., Rezayat, S.M., Falahati, M., 2019. J. Mol. Liq. 278, 130–144.

Baghayeri, M., Alinezhad, H., Tarahomi, M., Fayazi, M., Ghanei-Motlagh, M., Maleki, B., 2019. Appl. Surf. Sci. 478, 87–93.

Bai, J., Sun, C., Jiang, X., 2016. Anal. Bioanal. Chem. 408, 4705–4714.

Bai, Z., Dong, W., Ren, Y., Zhang, C., Chen, Q., 2018. Langmuir 34, 2235–2244.

Bai, Z., Li, G., Liang, J., Su, J., Zhang, Y., Chen, H., Huang, Y., Sui, W., Zhao, Y., 2016. Biosens. Bioelectron. 82, 185–194.

Braik, M., Zamfir, L.G., Rotariu, L., Curutiu, C., Chifiriuc, M.C., Ali, M. Ben, Bala, C., 2018. Sensors Actuators, B Chem. 273, 298–304.

Cheng, C., Zhang, C., Gao, X., Zhuang, Z., Du, C., Chen, W., 2018. Anal. Chem. 90, 1983–1991.

David, M., Barsan, M.M., Brett, C.M.A., Florescu, M., 2018. Sensors Actuators, B Chem. 255, 3227–3234.

de Fátima Cardoso Soares, M., de Oliveira Farias, E.A., da Silva, D.A., Eiras, C., 2016. J. Mater. Sci. 51, 7093–7107.

Deepalakshmi, T., Tran, D.T., Kim, N.H., Chong, K.T., Lee, J.H., 2018. ACS Appl. Mater. Interfaces 10, 35847–35858.

Dong, S., Zhang, D., Suo, G., Wei, W., Huang, T., 2016. Anal. Chim. Acta 934, 203–211.

Dong, W., Ren, Y., Bai, Z., Yang, Y., Wang, Z., Zhang, C., Chen, Q., 2018. Talanta 189, 79–85.

Eguílaz, M., Ferreyra, N.F., Rivas, G.A., 2014. Electroanalysis 26, 2434–2444.

Eguílaz, M., Gutiérrez, A., Rivas, G., 2016. Sensors Actuators B Chem. B Chem. 225, 74–80.

Eguílaz, M., Venegas, C.J., Gutiérrez, A., Rivas, G.A., Bollo, S., 2016b. Microchem. J. 128, 161–165.

Fu, Y., Huang, D., Li, C., Zou, L., Ye, B., 2018. Anal. Chim. Acta 1014, 10–18.

Gao, L., Zhuang, J., Nie, L., Zhang, J., Zhang, Y., Gu, N., Wang, T., Feng, J., Yang, D., Perrett, S., Yan, X., 2007. Nat. Nanotechnol. 2, 577–583.

Golchin, J., Golchin, K., Alidadian, N., Ghaderi, S., Eslamkhah, S., Eslamkhah, M., Akbarzadeh, A., 2017. Artif. Cells, Nanomedicine Biotechnol. 45, 1069–1076.

Gong, C., Chen, J., Song, Y., Sun, M., Song, Y., Guo, Q., Wang, L., 2016. Anal. Methods 8, 1513–1519.

Guler, M., Dilmac, Y., 2019. J. Electroanal. Chem. 834, 49–55.

Guler, M., Turkoglu, V., Bulut, A., Zahmakiran, M., 2018. Electrochim. Acta 263,

118–126.

Guo, Q., Liu, L., Wu, T., Wang, Q., Wang, H., Liang, J., Chen, S., 2018. Electrochim. Acta 281, 517–524.

Guo, Q., Liu, L., Zhang, M., Hou, H., Song, Y., Wang, H., Zhong, B., Wang, L., 2017. Biosens. Bioelectron. 92, 654–660.

Gutierrez, F.A., Gonzalez-Dominguez, J.M., Ansón-Casaos, A., Hernández-Ferrer, J., Rubianes, M.D., Martínez, M.T., Rivas, G., 2017. Sensors Actuators B Chem. 249, 506–514.

Gutierrez, F.A., Mazario, E., Menéndez, N., Herrasti, P., Rubianes, M.D., Zagal, J.H., Yañez, C., Rivas, G.A., Bollo, S., Recio, F.J., 2018. Electroanalysis 30, 1613–1618.

Gutierrez, F.A., Rubianes, M.D., Rivas, G.A., 2019. Anal. Chim. Acta 1065, 12–20.

Gutierrez, F., Rubianes, M.D., Rivas, G.A., 2012. Sensors Actuators, B Chem. 161, 191–197.

Hassan, M., Jiang, Y., Bo, X., Zhou, M., 2018. Talanta 188, 339–348.

Huang, B., Wang, Y., Lu, Z., Du, H., Ye, J., 2017. Sensors Actuators, B Chem. 252, 1016–1025.

Huang, Y., Xue, Y., Zeng, J., Li, S., Wang, Z., Dong, C., Li, G., Liang, J., Zhou, Z., 2018. Mater. Sci. Eng. C 92, 590–598.

Jomma, E.Y., Ding, S.N., 2016. Sensors (Switzerland) 16, 243–253.

Karthikeyan, C., Ramachandran, K., Sheet, S., Yoo, D.J., Lee, Y.S., Satish Kumar, Y., Kim, A.R., Gnana Kumar, G., 2017. ACS Sustain. Chem. Eng. 5, 4897–4905.

Li, C., Wu, R., Zou, J., Zhang, T., Zhang, S., Zhang, Z., Hu, X., Yan, Y., Ling,

X., 2018. Biosens. Bioelectron. 116, 81–88.

Li, C., Zhang, T., Zhao, J., Liu, H., Zheng, B., Gu, Y., Yan, X., Li, Y., Lu, N., Zhang, Z., Feng, G., 2017. ACS Appl. Mater. Interfaces 9, 2984–2994.

Li, D., Meng, L., Xiao, P., Jiang, D., Dang, S., Chen, M., 2017. J. Electroanal. Chem. 791, 23–28.

Liu, J.X., Ding, S.N., 2017. Sensors Actuators, B Chem. 251, 200–207.

Maduraiveeran, G., Sasidharan, M., Ganesan, V., 2018. Biosens. Bioelectron. 103, 113–129.

Manoj, D., Theyagarajan, K., Saravanakumar, D., Senthilkumar, S., Thenmozhi, K., 2018. Biosens. Bioelectron. 103, 104–112.

Mayuri, P., Saravanan, N., Senthil Kumar, A., 2017. Electrochim. Acta 240, 522–533.

Moozarm Nia, P., Woi, P.M., Alias, Y., 2017. Appl. Surf. Sci. 413, 56–65.

Ning, Y.N., Xiao, B.L., Niu, N.N., Moosavi-Movahedi, A.A., Hong, J., 2019. Polymers (Basel). 11, 115.

Olivieri, A.C., Goicoechea, H.C., 2007. UNL, Santa Fe, Argentina.

Primo, E.N., Cañete-Rosales, P., Bollo, S., Rubianes, M.D., Rivas, G.A., 2013. Colloids Surfaces B Biointerfaces 108, 329–336.

Primo, E.N., Oviedo, M.B., Sánchez, C.G., Rubianes, M.D., Rivas, G.A., 2014. Bioelectrochemistry 99, 8–16.

Rafighi, P., Tavahodi, M., Haghighi, B., 2016. Sensors Actuators, B Chem. 232, 454–461.

Rama, E.C., Costa-García, A., Fernández-abedul, T., 2017. Biosens. Bioelectron. 88, 34–40.

Roushani, M., Bakyas, K., Zare Dizajdizi, B., 2016. Mater. Sci. Eng. C 64, 54–

60.

Saglam, Ö., KIzIlkaya, B., Uysal, H., Dilgin, Y., 2016. Talanta 147, 315–321.

Sakslund, H., Wang, J., Lu, F., Hammerich, O., 1995. J. Electroanal. Chem. 397, 149–155.

Shahnavaz, Z., Abd Hamid, S.B., 2017. Appl. Surf. Sci. 407, 379–385.

Song, Y., Lu, X., Li, Y., Guo, Q., Chen, S., Mao, L., Hou, H., Wang, L., 2016. Anal. Chem. 88, 1371–1377.

Tang, H., Cai, D., Ren, T., Xiong, P., Liu, Y., Gu, H., Shi, G., 2019. Anal. Biochem. 567, 63–71.

Wang, C., Huang, S., Luo, L., Zhou, Y., Lu, X., Zhang, G., Ye, H., Gu, J., Cao, F., 2019. J. Electroanal. Chem. 835, 178–185.

Wang, H., Li, S., Si, Y., Zhang, N., Sun, Z., Wu, H., Lin, Y., 2014. Nanoscale 6, 8107–8116.

Wang, L., Li, J., Feng, M., Min, L., Yang, J., Yu, S., Zhang, Y., Hu, X., Yang, Z., 2017. Biosens. Bioelectron. 96, 220–226.

Wang, Z.-X., Wang, J.-Y., Yu, X.-H., Kong, F.-Y., Wang, W.-J., Lv, W.-X., Ge, L., Wang, W., 2017. Sensors Actuators B Chem. 246, 726–733.

Wei, H., Wang, E., 2013. Chem. Soc. Rev. 42, 6060–6093.

Wu, J., Li, S., Wei, H., 2018. Nanoscale Horizons 3, 367–382.

Wu, J., Wang, X., Wang, Q., Lou, Z., Li, S., Zhu, Y., Qin, L., Wei, H., 2019. Chem. Soc. Rev. 48, 1004–1076.

Xia, H., Kitazumi, Y., Shirai, O., Kano, K., 2017. Anal. Sci. 33, 839–844.

Xu, Q., Yuan, H., Dong, X., Zhang, Y., Asif, M., Dong, Z., He, W., Ren, J., Sun, Y., Xiao, F., 2018. Biosens. Bioelectron. 107, 153–162.

Yang, H., Gong, C., Miao, L., Xu, F., 2017. Int. J. Electrochem. Sci. 12, 4958–

4969.

Ye, H., Mohar, J., Wang, Q., Catalano, M., Kim, M.J., Xia, X., 2016. Sci. Bull. 61, 1739–1745.

Zhang, J., Yu, X., Guo, W., Qiu, J., Mou, X., Li, A., Liu, H., 2016. Nanoscale 8, 9382–9389.

Zhang, T., Gu, Y., Li, C., Yan, X., Lu, N., Liu, H., Zhang, Z., Zhang, H., 2017. ACS Appl. Mater. Interfaces 9, 37991–37999.

Zhang, Y., Xiao, J., Sun, Y., Wang, L., Dong, X., Ren, J., He, W., Xiao, F., 2018. Biosens. Bioelectron. 100, 453–461.

Zhou, Y., Li, C., Hao, Y., Ye, B., Xu, M., 2018. Talanta 188, 282–287.

Zhu, C., Yang, G., Li, H., Du, D., Lin, Y., 2015. Anal. Chem. 87, 230–249.

Highlights-RIVAS ET AL

- The nanohybrid MWCNTs-Av/RuNPs presents enhanced peroxidase-like activity and site-specific biorecognition properties.
- The combination of MWCNT-avidin/RuNPs allows the synergic catalytic reduction of $H_2O_2$.
- GCE/MWCNT-avidin/RuNPs makes possible the highly sensitive quantification of $H_2O_2$.
- GCE/MWCNT-avidin/RuNPs/biotin-GOx works as a highly sensitive pseudo-bienzymatic glucose biosensor.
- GCE/MWCNT-avidin/b-HRP is successfully used for detecting of glucose in soft drinks.

The authors of the manuscript "**Designing electrochemical interfaces based on nanohybrids of avidin functionalized-carbon nanotubes and ruthenium nanoparticles as peroxidase-like nanozyme with supramolecular recognition properties for site-specific anchoring of biotinylated residues**", Pablo Gallay, Marcos Eguílaz and Gustavo Rivas declare that there are no conflicts of interest.

ROLE OF THE AUTHORS:

Dr. Pablo Gallay performed the experimental work.

Dr. Marcos Eguílaz supervised the experimental work, analyzed the results and wrote the first version of the manuscript and participated in the final redaction of the corrected manuscript.

Dr. Gustavo Rivas supervised the whole work, is the responsible for the idea of the work, is the responsible for the grant, and wrote the final version of the manuscript and the corrected version of the manuscript.

**Declaration of interests**

☒ The authors declare that they have no known competing financial interests or personal relationships that could have appeared to influence the work reported in this paper.

☐The authors declare the following financial interests/personal relationships which may be considered as potential competing interests: